Smart Structures and Systems, *Vol. 14, No. 6 (2014) 1105-1129*
DOI: http://dx.doi.org/10.12989/sss.2014.14.6.1105

Model updating with constrained unscented Kalman filter for hybrid testing

Bin Wu*[1,2] and Tao Wang[1,2,3]

[1]*Key Lab of Structures Dynamic Behavior and Control (Harbin Institute of Technology), Ministry of Education, Harbin, 150090, China*
[2]*Harbin Institute of Technology, Harbin, China*
[3]*Heilongjiang University of Science and Technology, Harbin, China*

(Received March 3, 2014, Revised May 15, 2014, Accepted June 10, 2014)

Abstract. The unscented Kalman filter (UKF) has been developed for nonlinear model parametric identification, and it assumes that the model parameters are symmetrically distributed about their mean values without any constrains. However, the parameters in many applications are confined within certain ranges to make sense physically. In this paper, a constrained unscented Kalman filter (CUKF) algorithm is proposed to improve accuracy of numerical substructure modeling in hybrid testing. During hybrid testing, the numerical models of numerical substructures which are assumed identical to the physical substructures are updated online with the CUKF approach based on the measurement data from physical substructures. The CUKF method adopts sigma points (i.e., sample points) projecting strategy, with which the positions and weights of sigma points violating constraints are modified. The effectiveness of the proposed hybrid testing method is verified by pure numerical simulation and real-time as well as slower hybrid tests with nonlinear specimens. The results show that the new method has better accuracy compared to conventional hybrid testing with fixed numerical model and hybrid testing based on model updating with UKF.

Keywords: model updating; real-time hybrid testing; unscented Kalman filter; bound constraint

1. Introduction

Real-time hybrid testing is a combination of numerical simulation and physical testing in real-time, which is increasingly being recognized as a powerful emerging technique that offers the opportunity for evaluation of large scale civil structures subjected to dynamic loading. In recent decades, a great deal of progress has been made in real-time hybrid testing such as numerical integration algorithms, loading control methods, actuator delay compensation and testing error analysis (Nakashima *et al*. 1992, Dorka 2002, Bayer *et al*. 2005, Jung and Shing 2006, Wu *et al*. 2007, Bursi *et al*. 2008, Ahmadizadeh *et al*. 2008, Mercan *et al*. 2008, Carrion *et al*. 2008, Mosqueda *et al*. 2007). However, researchers generally might still encounter a number of difficulties when conducting hybrid testing for complex structures like high-rise buildings or large-scale bridges. One of the challenging issues is how to model the numerical substructure, when the whole structure exhibit strong nonlinearity subjected to extreme loading like strong

*Corresponding author, Professor, E-mail: bin.wu@hit.edu.cn

http://www.techno-press.org/?journal=sss&subpage=8 ISSN: 1738-1584 (Print), 1738-1991 (Online)

earthquake and it is not economically realistic to physically test all the critical parts of the structure. Even sophisticated finite element modeling is available, people still often argue that there is little sense to do physical tests if the finite element approach is reliable.

A convenient way to improve the reliability of numerical modeling in hybrid testing is online model updating based on test data from experimental substructures. Yang and Nakano (2005) developed a neural network algorithm to predict online the restoring force of numerical substructures using experimental data in a hybrid test. But the neural network method has a number of difficulties to be overcome when it is to be used for large scale structures; these difficulties include lack of physical meaning and adaptability of the network trained based on a selected set of data. Wang *et al*. (2011) used least square method to update the elasto-plastic model, and its effectiveness was verified by actual tests with steel buckling-restrained braces as physical substructures. For the sake of computational efficiency, the parameters of the bilinear model were actually estimated using linear regression with least square criterion. But the bilinear model is somewhat oversimplified for civil engineering structures, and direct use of least square method for nonlinear parameter identification will face the challenge of computational efficiency.

Kalman filter provides a general framework for recursive estimation of system states or parameters for linear systems. It may be extended to be applied to nonlinear systems through so called extended Kalman filter (EKF) based on linearization. The deficiency for highly nonlinear systems of EKF can be relieved by unscented Kalman filter (UKF) (Julier *et al*. 2000). The core idea of UKF is to adopt unscented transform technique to propagate mean and covariance. Through unscented transform, which is a type of deterministic sampling approach, the mean and covariance of nonlinear transformation of a random variable have up to third-order accuracy (Julier *et al*. 2000, Simon 2006). The other advantage of UKF is its high computational efficiency, as it does not need to calculate Jacobian and Hessian matrices of a nonlinear model which is necessary in EKF. The UKF has been applied in civil engineering to update Bouc-Wen hysteresis model in real-time (Song and Dyke 2013a,b). For hybrid simulation, Zhang (2010) used UKF to update numerical model and its effectiveness was confirmed by numerical simulation as well as an actual test with a steel spring as the experimental substructure (Wang and Wu 2012). The UKF was also validated by Hashemi *et al*. (2014) in a hybrid test with a rotational spring as the nonlinear part of the physical substructure.

But the standard UKF does not take into account any constraint on state variables or parameters. The constraint can be viewed as a remediation for inaccurate system modeling which is often the case in practice. Many approaches have been developed for UKF of constrained problems or called constrained UKF (CUKF) in recent years (Vachhani *et al*. 2006, Kandepu *et al*. 2008, Kolas *et al*. 2009, Chatzi *et al*. 2010, Mandela *et al*. 2012). In this paper, an improved CUKF is proposed based on sample point replacement method, and is used for model updating in hybrid testing.

The remainder of this paper is organized as follows. The improved CUKF is proposed in Section2. Then the effectiveness of CUKF itself as a parameter estimation method (without application to hybrid simulation) is revealed through numerical simulation in Section 3, and the effect of CUKF applied to hybrid simulation is investigated numerically in Section 4. Finally, the effect of CUKF is validated with slower hybrid test in Section 5.1 and with real-time hybrid test in Section 5.2.

2. Improved constrained UKF

Compared to existing CUKF, the approach proposed in this paper features the following two aspects: (i) in prediction step, sigma points (i.e., sample point) violating bound constraints are moved onto the bounds, and the relevant sigma points within the boundary are moved correspondingly to retains the symmetry of the new set of sigma points; (ii) in correction step, the state updating equation is used to generate transformed sigma points, and those transformed sigma points that violate bound constraints are projected to constraints boundary only when the updated state estimate exceeds the boundary. The details of above proposals are described as follows.

Consider a nonlinear dynamic system described by following discrete state-space equation and measurement equation as

$$\mathbf{x}_{k+1} = f\left(\mathbf{x}_k, \mathbf{u}_k\right) + \mathbf{v}_k \tag{1}$$

$$\mathbf{y}_{k+1} = h\left(\mathbf{x}_{k+1}, \mathbf{u}_{k+1}\right) + \mathbf{w}_{k+1} \tag{2}$$

where $\mathbf{x} \in \mathrm{R}^n$ is the n-dimensional vector of system state, u_k is the known input, $\mathbf{y} \in \mathrm{R}^m$ is the m-dimensional vector of measurement, $\mathbf{v}$ and $\mathbf{w}$ are Gaussian white noises with zero mean and covariance matrices $\mathbf{Q}$ and $\mathbf{R}$, respectively, and k represents the k-th time step. The major task we want to accomplish is to estimate the system state, *i.e.*, calculate the mean as well as covariance of system state at the (k+1)-th step, based on the state estimation at the k-th step, measurements at the current (k+1)-th step, and the information on state constraints. Just like standard UKF method, improved constrained UKF also includes the prediction and correction steps.

2.1 Prediction step

Assume $\hat{\mathbf{x}}_{k|k}$ is the state estimate, i.e., the estimate of mean of state, and $\mathbf{P}_{k|k}$ the corresponding covariance matrix at the k-th step. According to the standard UKF, a set of 2n+1 sigma points $\mathbf{X}_{k|k,i}$ are chosen symmetrically about $\hat{\mathbf{x}}_{k|k}$ as

$$\mathbf{X}_{k|k,i} = \hat{\mathbf{x}}_{k|k}, \quad i = 0 \tag{3}$$

$$\mathbf{X}_{k|k,i} = \hat{\mathbf{x}}_{k|k} + \theta_{k,i}\mathbf{s}_{k,i}, \quad i = 1, 2, \cdots, 2n \tag{4}$$

where

$$\theta_{k,i} = \sqrt{(n+\kappa)}, \quad i = 1, 2, \cdots, 2n \tag{5}$$

$$\mathbf{s}_{k,i} = \left(\sqrt{\mathbf{P}_{k|k}}\right)_i, \quad i = 1, 2, \cdots, n \tag{6}$$

$$\mathbf{s}_{k,i} = -\left(\sqrt{\mathbf{P}_{k|k}}\right)_{i-n}, \quad i = n+1, n+2, \cdots, 2n \tag{7}$$

where $\left(\sqrt{\mathbf{P}_{k|k}}\right)_i$ represents the i-th column vector of the matrix square root of $\mathbf{P}_{k|k}$, and $\theta_{k,i}$ is a algorithmic parameter denoting the sampling step size. Associated weights of sigma points are computed with

$$W_{k,0} = \frac{\kappa}{n+\kappa} \tag{8}$$

$$W_{k,i} = \frac{1}{2(n+\kappa)}, \quad i = 1, 2, \cdots, 2n \tag{9}$$

κ is a scaling parameter which can be any number providing that $(n + \kappa) \neq 0$. If κ is a negative value, the covariance matrices may become indefinite in some cases (Julier *et al*. 2000).

In many applications of UKF as well as Kalman filter, the state estimates or sigma points exceed certain range and become physically meaningless as they evolve with time. The reason for this may be attributed to modeling errors or high noises. There are already a number of proposals to handle this issue. Mandela *et al*. (2012) describes several CUKF approaches, all of them except one are asymmetric replacement of sigma points. Asymmetric placement of sigma points may result in biased estimates. Unbiasedness can be retained if the symmetric scaled unscented transformation (Julier *et al*. 2002) is employed. However, when the distance between the sigma points and mean value is scaled by a factor α so that all the points are constrained within the state boundary, the weights are divided by α^2 correspondingly. Then weights may grow too large and cause numerical difficulty if the mean approaches the state boundary.

To avoid the numerical difficulty of scaled unscented transformation and retain the symmetry of sigma points, we propose a simple approach in which the sigma points violating bound constraints are placed back onto the bounds along the direction to the central sigma point, and at the same time the sigma points that are symmetry to those out of boundary are moved correspondingly so that the symmetry remains for the new set of sigma points. This is illustrated in Fig. 1(a) for two-dimension case. The proposed replacement of sigma points is different from the symmetric placement described by Mandela *et al*. (2012), where all the replaced sigma points have the same sampling step size θ relative to the central sigma point, which means that many pairs of replaced sigma points may fall into the boundary, contrasting that at least one point of each of these pairs falls on the boundary as proposed herein. The symmetric approach of Mandela *et al*. (2012) may lead to too large weight value when the mean value is very close to the boundary, which is similar to the scaled UKF.

The expressions of the proposed sigma point replacement are derived as follows. The sigma points are determined still using Eq. (4), but the sampling step size $\theta_{k,i}$ for those exceeding constrained bounds as well as their symmetric counterparts is calculated with following equation.

$$\theta_{k,i} = \theta_{k,n+i} = \min(\theta_{k,i}^{\mathrm{C}}, \theta_{k,n+i}^{\mathrm{C}}), \quad i = 1, 2, \cdots, n \tag{10}$$

where

$$\theta_{k,i}^{\mathrm{C}} = \min(\theta_{k,i}^{\mathrm{U}}, \theta_{k,i}^{\mathrm{L}}), \quad i = 1, 2, \cdots, 2n \tag{11}$$

$$\theta_{k,i}^{\mathrm{L}} = \min_{\substack{j=1:n \\ (\mathbf{s}_{k,i})_j < 0}} \left\{ \sqrt{(n+\kappa)}, \left[(\mathbf{x}_{\mathrm{L}})_j - (\hat{\mathbf{x}}_{k|k})_j \right] \Big/ (\mathbf{s}_{k,i})_j \right\}, \quad i = 1, 2, \cdots, 2n \tag{12}$$

$$\theta_{k,i}^{\mathrm{U}} = \min_{\substack{j=1:n \\ (\mathbf{s}_{k,i})_j > 0}} \left\{ \sqrt{(n+\kappa)}, \left[(\mathbf{x}_{\mathrm{U}})_j - (\hat{\mathbf{x}}_{k|k})_j \right] \Big/ (\mathbf{s}_{k,i})_j \right\}, \quad i = 1, 2, \cdots, 2n \tag{13}$$

$\mathbf{x}_{\mathrm{U}}$ and $\mathbf{x}_{\mathrm{L}}$ represent the upper and lower bound of constrained vectors, and the subscript j represents

the *j*-th element of corresponding vector.

The weights of all of sigma points are adjusted by using a linear weighting method with respect to corresponding sampling step $\theta_{k,i}$ proposed by Vachhani *et al.* (2006) and re-written in notations of this paper as

$$W_{k,0} = a\theta_{k,0} + b = b\ , \quad i = 0 \tag{14}$$

$$W_{k,i} = a\theta_{k,i} + b\ , \quad i = 1,2,\cdots,2n \tag{15}$$

where

$$a = \frac{2\kappa - 1}{2(n+\kappa)[S_k - (2n+1)\sqrt{n+\kappa}]} \tag{16}$$

$$b = \frac{1}{2(n+\kappa)} + \frac{2\kappa - 1}{2\sqrt{(n+\kappa)}[(2n+1)\sqrt{n+\kappa} - S_k]} \tag{17}$$

$$S_k = \sum_{i=1}^{2n} \theta_{k,i} \tag{18}$$

It can be shown that the proposed replacement of sigma points results in a first-order accuracy for the unscented transformation of mean value if κ = 0.5; the proof is given in Appendix A. Therefore, we set κ = 0.5 in this paper.

Each sigma point $\mathbf{X}_{k|k,i}$ is transformed through the state-space equation to yield sigma point of state prediction $\mathbf{X}_{k+1|k,i}$ as

$$\mathbf{X}_{k+1|k,i} = f\left(\mathbf{X}^{\mathrm{C}}_{k|k,i}\right), \quad i = 0,1,\cdots,2n\ . \tag{19}$$

Then the mean $\hat{\mathbf{x}}_{k+1|k}$ and its error covariance matrix $\mathbf{P}_{k+1|k}$ of the predicted state estimate are calculated according to the standard UKF method as

$$\hat{\mathbf{x}}_{k+1|k} = \sum_{i=0}^{2n} W_{k,i}\mathbf{X}_{k+1|k,i} \tag{20}$$

$$\mathbf{P}_{k+1|k} = \sum_{i=0}^{2n} W_{k,i}\left(\mathbf{X}_{k+1|k,i} - \hat{\mathbf{x}}_{k+1|k}\right)\left(\mathbf{X}_{k+1|k,i} - \hat{\mathbf{x}}_{k+1|k}\right)^{\mathrm{T}} + \mathbf{Q}_k \tag{21}$$

2.2 Correction step

In order to obtain the updated estimate $\hat{\mathbf{x}}_{k+1|k+1}$ and its covariance matrix $\mathbf{P}_{k+1|k+1}$ given new measurement $\mathbf{y}_{k+1}$, we first need to calculate the predicted measurement sigma points $\mathbf{Y}_{k+1|k,i}$, the mean $\hat{\mathbf{y}}_{k+1|k}$ and covariance matrix $\mathbf{P}_{\mathrm{yy},k+1|k}$ of predicted measurement and the cross covariance matrix $\mathbf{P}_{\mathrm{xy},k+1|k}$ according to the standard UKF method as

$$\mathbf{Y}_{k+1|k,i} = h(\mathbf{X}_{k+1|k,i})\ , \quad i = 0,1,\cdots,2n \tag{22}$$

$$\hat{\mathbf{y}}_{k+1|k} = \sum_{i=0}^{2n} W_{k,i} \mathbf{Y}_{k+1|k,i} \tag{23}$$

$$\mathbf{P}_{\mathrm{yy},k+1|k} = \sum_{i=0}^{2n} W_{k,i} \left(\mathbf{Y}_{k+1|k,i} - \hat{\mathbf{y}}_{k+1|k} \right) \left(\mathbf{Y}_{k+1|k,i} - \hat{\mathbf{y}}_{k+1|k} \right)^{\mathrm{T}} + \mathbf{R}_{k+1} \tag{24}$$

$$\mathbf{P}_{\mathrm{xy},k+1|k} = \sum_{i=0}^{2n} W_{k,i} \left(\mathbf{X}_{k+1|k,i} - \hat{\mathbf{x}}_{k+1|k} \right) \left(\mathbf{Y}_{k+1|k,i} - \hat{\mathbf{y}}_{k+1|k} \right)^{\mathrm{T}} \tag{25}$$

The Kalman filter gain can then be obtained through

$$\mathbf{K}_{k+1} = \mathbf{P}_{\mathrm{xy},k+1|k} \mathbf{P}_{\mathrm{yy},k+1|k}^{-1} \tag{26}$$

For unconstrained system states, the UKF method adopts state correction equation of the standard Kalman filter to calculate the mean and covariance of the corrected state. For the constrained state estimate, Vachhani *et al*. (2006) employs the sophisticated constrained nonlinear optimization method to calculate the mean and covariance at correction step. A more straight-forward way to deal with the constraining issue is to simply project the transformed sigma points onto the boundary if the updated estimate exceeds the constraint. In more details, the transformed sigma points are produced with Kalman updating equation as

$$\mathbf{X}_{k+1|k+1,i} = \mathbf{X}_{k+1|k,i} + \mathbf{K}_{k+1} \left(\mathbf{y}_{k+1} - \mathbf{Y}_{k+1|k,i} \right), \quad i = 0,1,\cdots,2n \tag{27}$$

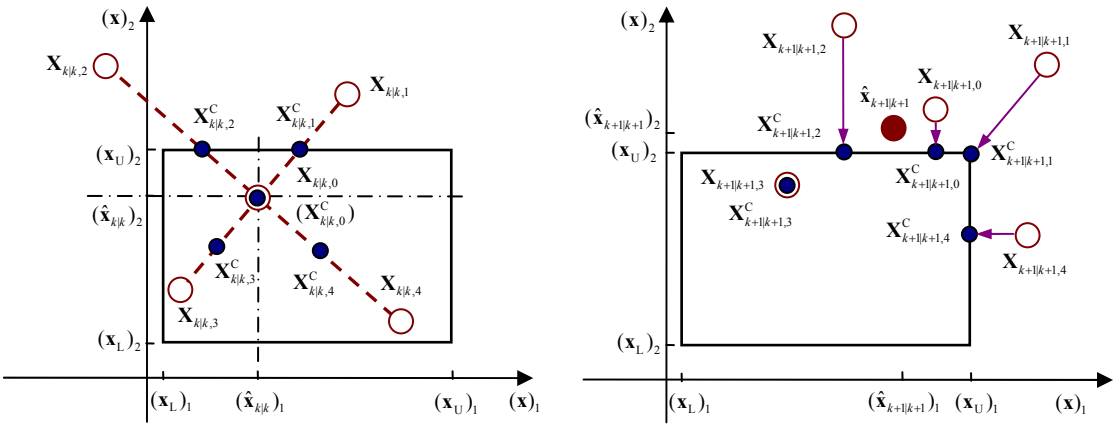

(a) Prediction step (b) Correction step

Fig. 1 Sigma points replacement with state constraints in CUKF

Note that the sigma points in Kolas *et al.* (2009) are augmented with process errors and measurement errors, although the expression of transformed sigma points therein is similar to Eq. (27). With $\mathbf{X}_{k+1|k+1,i}$ calculated by Eq. (27), the state update $\hat{\mathbf{x}}_{k+1|k+1}$ and its covariance $\mathbf{P}_{k+1|k+1}$ can be calculated using following equations.

$$\hat{\mathbf{x}}_{k+1|k+1} = \sum_{i=0}^{2n} W_{k,i} \mathbf{X}_{k+1|k+1,i} \tag{28}$$

$$\mathbf{P}_{k+1|k+1} = \sum_{i=0}^{2n} W_{k,i} \left(\mathbf{X}_{k+1|k+1,i} - \hat{\mathbf{x}}_{k+1|k+1}\right)\left(\mathbf{X}_{k+1|k+1,i} - \hat{\mathbf{x}}_{k+1|k+1}\right)^{\mathrm{T}} + \mathbf{Q}_k + \mathbf{K}_{k+1}\mathbf{R}_{k+1}\mathbf{K}_{k+1}^{\mathrm{T}} \tag{29}$$

It can be proved that the above equations give exactly the same result of updated mean and covariance with the standard UKF. The proof for the covariance expression is given in Appendix B of this paper, while that for the mean is the same as in Kolas *et al.* (2009).

If the state mean estimate violates the bound constraints, the sigma points outside boundary are projected to the boundary, as shown in Fig. 1(b). Let $\mathbf{X}^{\mathrm{C}}_{k+1|k+1,i}$ denote the replaced sigma point, then its substituting $\mathbf{X}_{k+1|k+1,i}$ in Eqs. (28) and (29) gives the corrected state update and its covariance.

3. Numerical example of model parametric estimation

Consider the Bouc-Wen hysteretic model described by (Wen 1976)

$$r = \alpha k d + (1-\alpha) k z \tag{30}$$

$$\dot{z} = v\text{-}\beta |v||z|^{n-1} z - \gamma v |z|^{n} \tag{31}$$

where r is restoring force; d, v, z are displacement, velocity and hysteretic displacement, respectively; k, α, β, γ and n are parameters controlling the size and shape of hysteretic loop; k and α can be interpreted as initial stiffness and second stiffness coefficient, respectively, for $n = \infty$.

The parameters to be estimated are k, β, γ, n and α. With z as an intermediate variable, the system state vector is defined as $\mathrm{x} = [x_1, x_2, x_3, x_4, x_5, x_6]^{\mathrm{T}} = [z, k, \beta, \gamma, n, \alpha]^{\mathrm{T}}$, the system measurement is restoring force, i.e., $y = r$, and the input is displacement d and velocity v. Then continuous state equation is expressed as

$$\dot{\mathbf{x}} = \begin{bmatrix} \dot{x}_1 \\ \dot{x}_2 \\ \dot{x}_3 \\ \dot{x}_4 \\ \dot{x}_5 \\ \dot{x}_6 \end{bmatrix} = \begin{bmatrix} \dot{z} \\ \dot{k} \\ \dot{\beta} \\ \dot{\gamma} \\ \dot{n} \\ \dot{\alpha} \end{bmatrix} = g(\mathbf{x}, v) + \dot{\mathbf{v}} = \begin{bmatrix} v - x_3 |v| |x_1|^{x_5 - 1} x_1 - x_4 v |x_1|^{x_5} \\ 0 \\ 0 \\ 0 \\ 0 \\ 0 \end{bmatrix} + \dot{\mathbf{v}} \tag{32}$$

By applying a numerical integration method to the above equation, the discrete state equation can be expressed as

$$\mathbf{x}_{k+1} = f\left(\mathbf{x}_k, \mathbf{u}_k\right) + \mathbf{v}_k = \mathbf{x}_k + \int_{k\Delta t}^{(k+1)\Delta t} \mathrm{g}(\mathbf{x}(\tau), v_k)\mathrm{d}\tau + \mathbf{v}_k \tag{33}$$

and the measurement equation is expressed as

$$y_{k+1} = r_{k+1} = h\left(\mathbf{x}_{k+1}, \mathbf{u}_{k+1}\right) + w_{k+1} = x_{6,k+1}x_{2,k+1}d_{k+1} + (1 - x_{6,k+1})x_{2,k+1}x_{1,k+1} + w_{k+1} \tag{34}$$

Ikhouane *et al*. (2007) have given parameter constraints of the classic Bouc-Wen model in terms of the bounded input-bounded output (BIBO) stability requirements. The model output can be unstable, for $\beta + \gamma < 0$, $\beta < 0$ or $n < 1$. Meanwhile, the hysteretic model will lose the actual physical meaning if the initial stiffness $k < 0$ and the second stiffness coefficient $\alpha > 1$ for structural materials typical of softening behavior. So, the bound constraints of the parameters for CUKF are $k \geq 0$, $\beta \geq 0$, $\gamma \geq -\beta$, $n \geq 1$, and $0 \leq \alpha \leq 1$.

The true values of the parameters are k = 135 kN/mm, β = 0.2, γ = 0.2, n = 1 and α = 0.02, but their initial guess are k = 115 kN/mm, β = 0.5, γ = 0.5, n = 2 and α = 0.1. The initial value of z is zero. The measurement noise w_{k+1} is the discrete Gaussian white noise whose standard deviation is 2% of that of true restoring force, which is equal to 0.84% of the peak restoring force. The observation noise covariance R_{k+1} is assumed 1.5 kN^2, and the process noise covariance $Q_k = 10^{-6}$ I_6, and the initial state estimate error covariance P_0 = diag (10^{-6}, 10, 10, 10, 10^{-2}, 10^{-2}). The displacement input is taken from data of a previous hybrid test with BRB (Wang *et al.* 2011), and the velocity input is calculated with forward difference method. The time histories of the inputs are shown in Fig. 2.

The parameters as well as intermediate variable z with CUKF and UKF are shown in Fig. 3. It is seen that all the parameter estimates approach true values at the end of time. Compared with the UKF method, the fluctuation of all the parameters except n is significantly reduced at the early stage and the speed of convergence of parameters n and α are increased when the CUKF is employed.

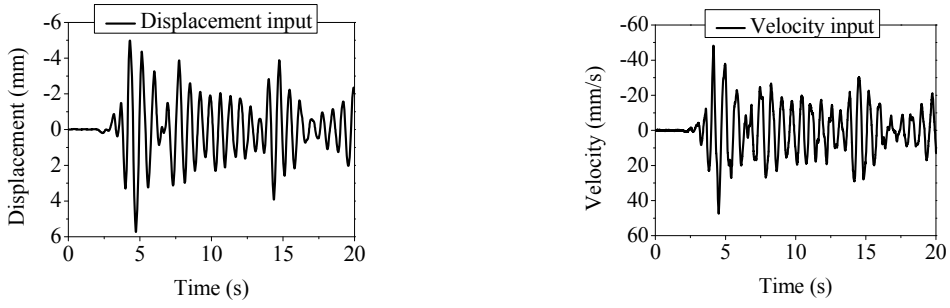

(a) Displacement input (b) Velocity input

Fig. 2 Displacement and velocity inputs of Bouc-Wen model

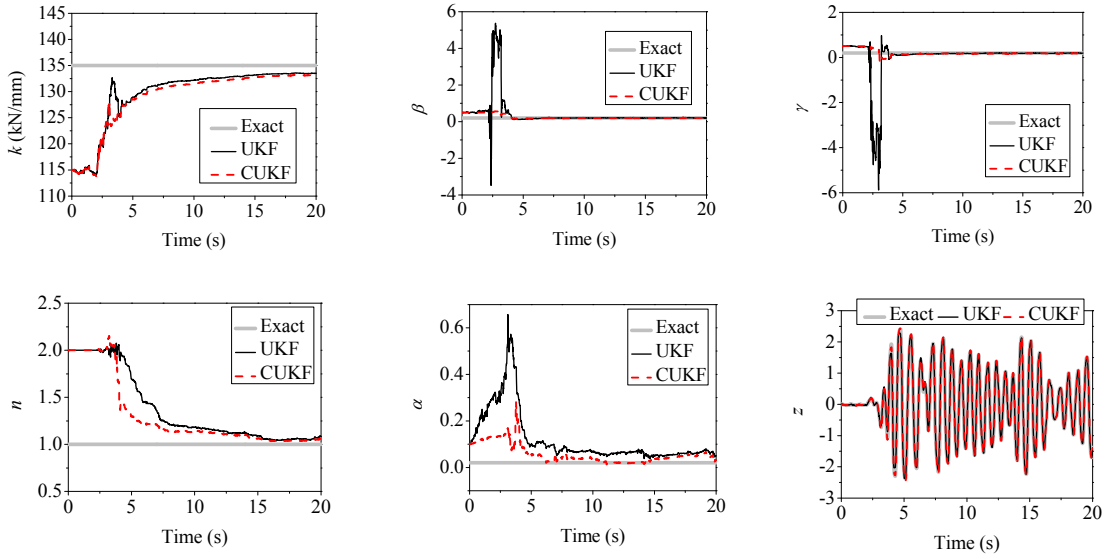

Fig. 3 Estimated parameters of Bouc-Wen model

The restoring force r, elastic force $r_e = \alpha kd$, and hysteretic force $r_h = (1-\alpha)kz$ with CUKF and UKF are compared with corresponding measurement and exact value, as shown in Figs. 4-6. The responses with initial guess values of the model parameters are also listed and denoted by "Initial" in these figures. For quantitative evaluation of the model updated errors, the Root Mean Square Deviation (RMSD) and the Normalized Relative Errors (NRE) are defined respectively as

$$\mathrm{RMSD}_k = \sqrt{\sum_{i=1}^{k}\left(F_i - F_i^{\mathrm{true}}\right)^2 \Big/ \sum_{i=1}^{k}\left(F_i^{\mathrm{true}}\right)^2} \tag{35}$$

$$\mathrm{NRE}_k = \left(F_k - F_k^{\mathrm{true}}\right) \Big/ \max_{i=1,\ldots,N}\left(r_i^{\mathrm{true}}\right) \tag{36}$$

RMSD_k can be interpreted as average relative error up to the k-th step while NRE_k can be thought of as the instantaneous relative error at the k-th step. The RMSDs of the restoring force, elastic force and hysteretic force are shown in Figs. 4(b), 5(b) and 6(b), respectively. The NREs are shown in Figs. 4(c), 5(c) and 6(c).

Fig. 4 shows that the restoring force can be well approximated by both UKF and CUKF. However, the errors of components of the restoring force, i.e., the elastic force and hysteretic force, are significantly reduced by CUKF compared to UKF, which is seen from Figs. 5 and 6. The RMSDs and NREs of both CUKF and UKF are much smaller than those of measurement as shown in Figs. 4(b) and 4(c), indicating a good noise filtering effects of the two methods.

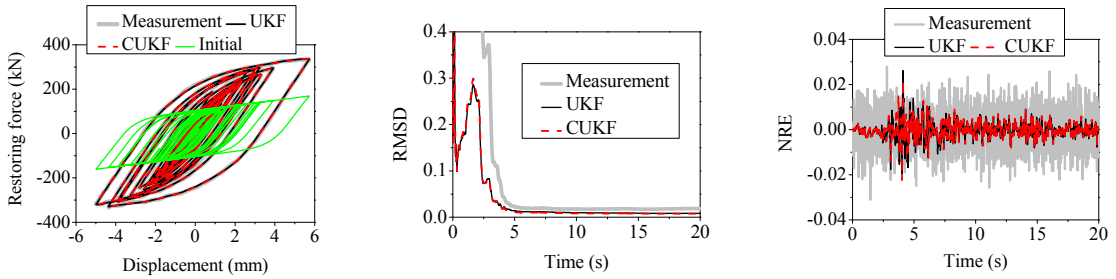

(a) Restoring force (b) RMSD (c) NRE

Fig. 4 Restoring forces and error responses

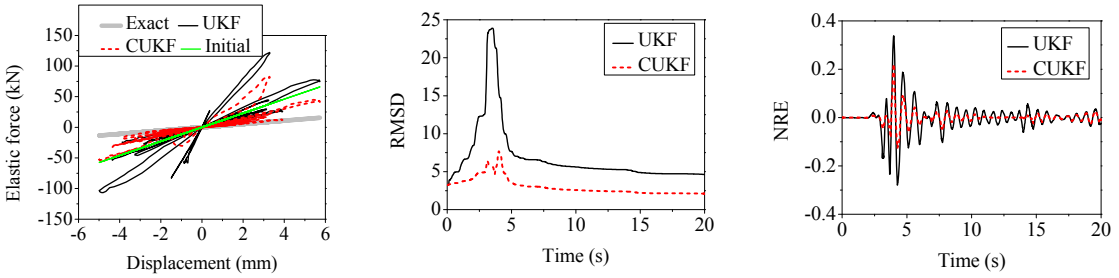

(a) Elastic force r_e (b) RMSD (c) NRE

Fig. 5 Elastic forces and errors responses

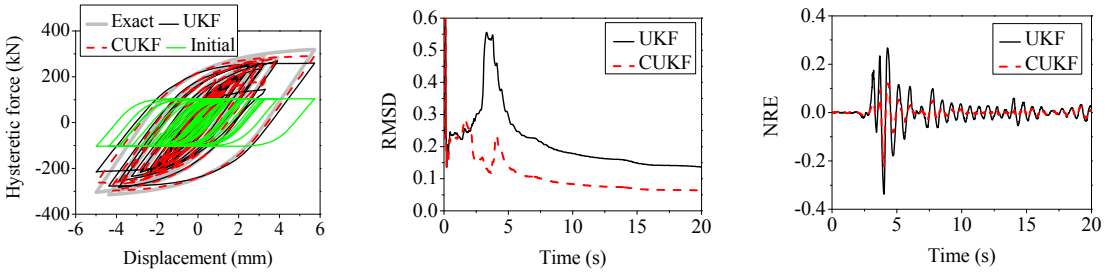

(a) Hysteretic force r_h (b) RMSD (c) NRE

Fig. 6 Hysteretic forces and errors responses

4. Numerical simulation of hybrid testing with model updating

Consider a structure of two-degree-of-freedom as shown in Fig. 7. For hybrid testing, the restoring force of the first degree of freedom is selected as physical substructure, and the remainder of the system is numerical substructure. With the inter-story responses as unknowns, the equation of motion is established as

$$\begin{bmatrix} m_1+m_2 & m_2 \\ m_2 & m_2 \end{bmatrix} \begin{Bmatrix} a_{k+1}^{\mathrm{E}} \\ a_{k+1}^{\mathrm{N}} \end{Bmatrix} + \begin{bmatrix} c_1 & 0 \\ 0 & c_2 \end{bmatrix} \begin{Bmatrix} v_{k+1}^{\mathrm{E}} \\ v_{k+1}^{\mathrm{N}} \end{Bmatrix} + \begin{Bmatrix} r_{k+1}^{\mathrm{E}}(d_{k+1}^{\mathrm{E}}) \\ r_{k+1}^{\mathrm{N}}(d_{k+1}^{\mathrm{N}}) \end{Bmatrix} = -\begin{bmatrix} m_1+m_2 & m_2 \\ m_2 & m_2 \end{bmatrix} \begin{Bmatrix} 1 \\ 0 \end{Bmatrix} a_{\mathrm{g},k+1} \tag{37}$$

or in a more compact form as

$$\mathbf{M}\mathbf{a}_{k+1} + \mathbf{C}\mathbf{v}_{k+1} + \mathbf{r}_{k+1} = \mathbf{F}_{k+1} \tag{38}$$

where a, v and d are inter-story acceleration, velocity and displacement, respectively; a_{g} is the acceleration of ground motion; r is the restoring force with Bouc-Wen model; the superscript E represents the physical substructure, and N represents the numerical substructure. We assume the numerical substructure has the same model of restoring force as experimental substructure. In hybrid testing, the parameters of the experimental substructure are estimated at each time step of numerical integration using test data and UKF or CUKF methods described in last two sections, and then the numerical substructure is updated at the same step with these parameter estimates.

The masses at the two degrees of freedom are $m_1 = m_2 = 0.2\times10^6$ kg, the elastic stiffness of the structure are $k_1 = k_2 = 135$ kN/mm, and the viscous damping coefficients are $c_1 = c_2 = 0.3$ kN/(mm/s). The resulting structural periods are $T_1 = 0.3913$ s and $T_2 = 0.1495$ s, and damping ratios are $\zeta_1 = 0.0178$ and $\zeta_2 = 0.0467$.

The seismic input is El Centro (NS 1940) earthquake record which peak acceleration scaled to 1000 mm/s^2. The fourth-order Runge-Kutta method is used for numerical integration with time interval of 0.01s. The standard deviation of measurement noise w_{k+1} is 2.4% of that of true restoring force, which is equal to 0.8% of the peak restoring force. The parameters for UKF and CUKF are the same as the numerical example in last section. To avoid large errors or even possible divergent responses with UKF, the estimated parameters exceeding constraints take boundary values for numerical substructure updating in this and next sections.

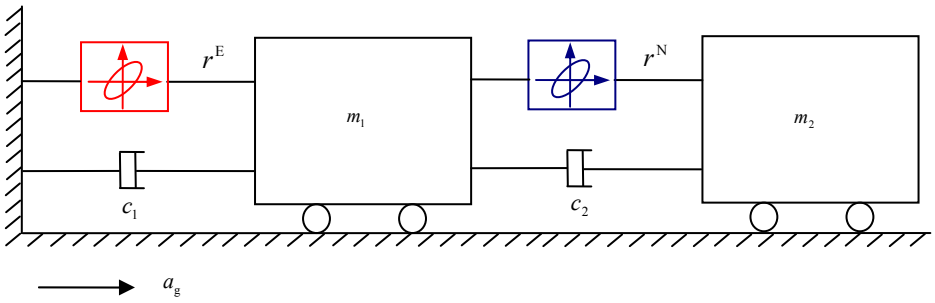

Fig. 7 Schematic of two-degree-of-freedom nonlinear system

The parameter identification results are shown in Fig. 8; the restoring force and its components of the experimental substructure are as shown in Fig. 9. Here again we see the advantage of CUKF over UKF in terms of parameter fluctuation and convergence speed; the CUKF has less error of elastic and hysteretic forces than UKF.

The restoring force and inter-story displacement of the numerical substructure are shown in Figs. 10 and 11. The RMSDs of the restoring force and inter-storey displacement of the numerical substructure are shown in Fig. 12. It is clearly seen from Figs. 10-12 that the responses have large errors without model updating; CUKF have fewer errors of displacement and restoring force than UKF. Comparison of Figs. 9(a) and 10 shows that the CUKF exhibits more significant effect on numerical substructure response than experimental substructure response. This may be attributed to parameter fluctuations at the early stage of the time history. The parameter fluctuations do not affect experimental substructure much because the optimal nature of UKF and CUKF drives the restoring force calculated with estimated parameters to track test data of experimental substructure as close as possible. But this is not the case for numerical substructure.

The numerical simulations are carried out on a laptop with CPU of 2.2GHz. The total computation time is about 2s for various cases with input of 20s in last section, and 3s for input of 30s in this section.

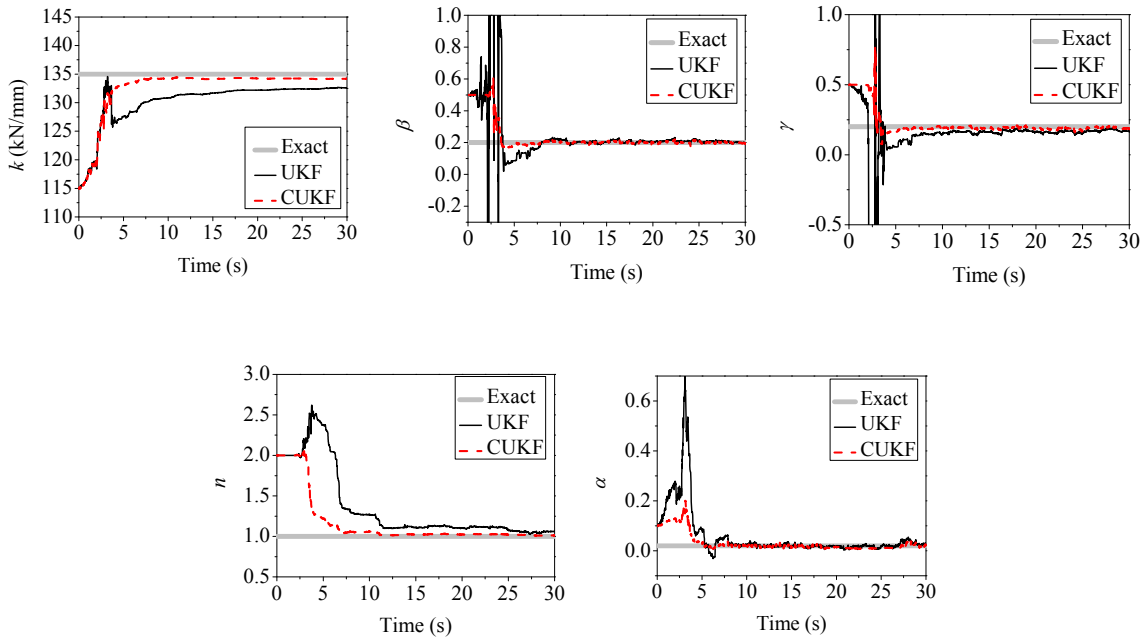

Fig. 8 Estimated parameters of hysteretic model

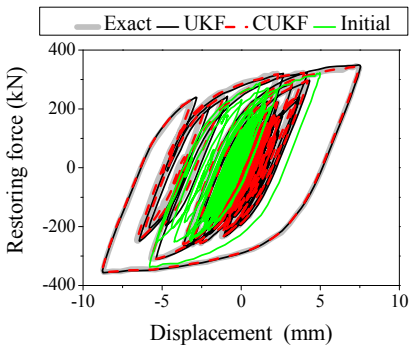

(a) Total restoring force

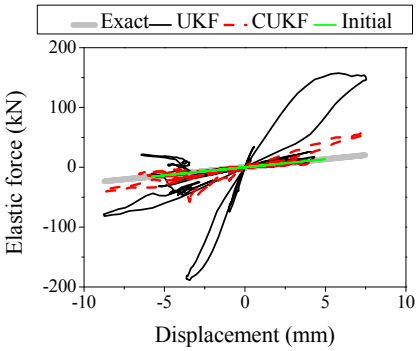

(b) Elastic force

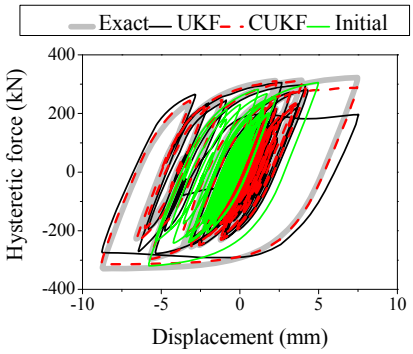

(c) Hysteretic force

Fig. 9 Restoring force and its components of the experimental substructure

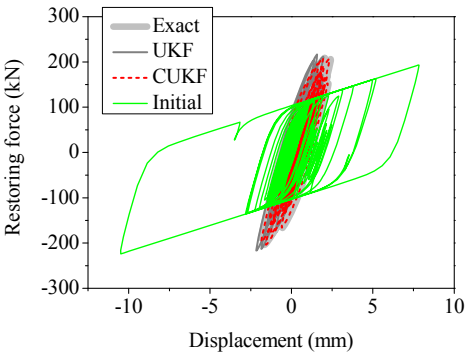

(a) Over-all view

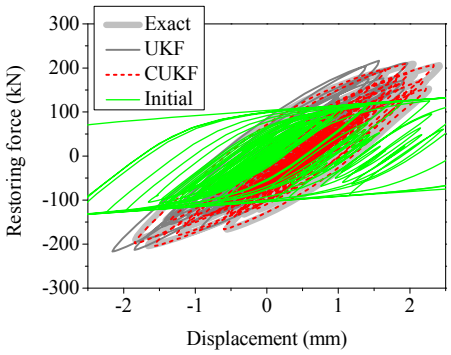

(b) Close-up view

Fig. 10 Hysteretic loops of the numerical substructure

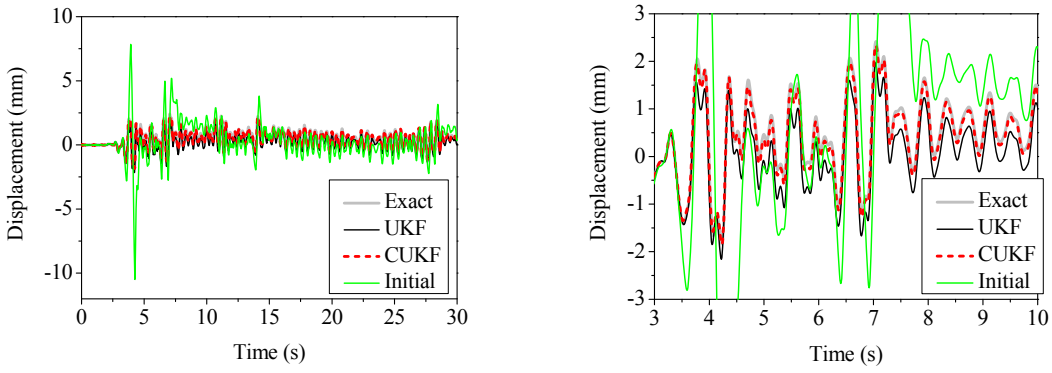

(a) Over-all view (b) Close-up view

Fig. 11 Inter-story displacement of the numerical substructure

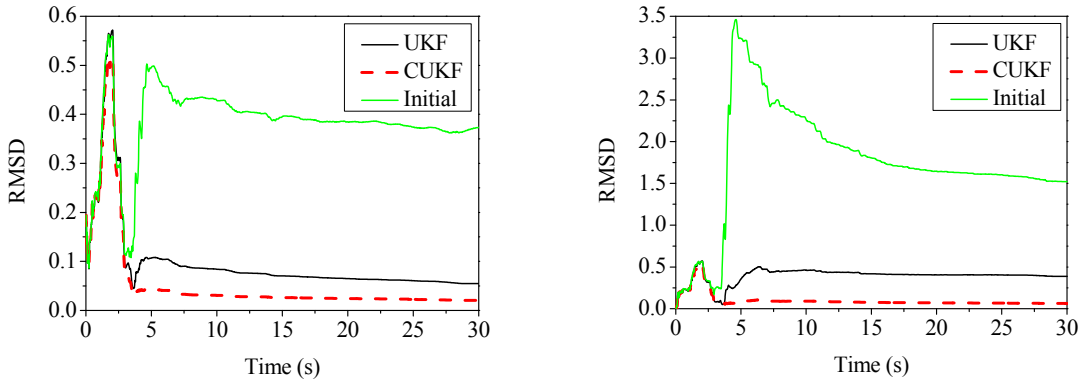

(a) Restoring force (b) Inter-storey displacement

Fig. 12 RMSD of restoring force and inter-storey displacement of the numerical substructure

5. Experimental verification

A series of hybrid tests in increased time scale and in real time are conducted at Structural and Seismic Testing Center of Harbin Institute of Technology (Wang and Wu 2014). Presented below are the test of a two-degree-of-freedom structure in slowed down time scale and that of a single-degree-of- freedom structure in real time. In both cases, the experimental substructure is a buckling restrained brace.

5.1 Hybrid test in increased time scale

The test structure is a two-story frame structure incorporating two all-steel buckling-restrained braces (BRBs) as shown in Fig. 13. The BRB on the first floor is selected as physical substructure and taken out into the test rig with a MTS actuator as shown in Fig. 14; the remainder of the

structure is numerically modeled in the CPU of dSPACE real-time simulation system. The BRB specimen has a steel core plate with the length of 1080 mm and cross section of 72×12 mm. The outer restraining part is a square steel tube with a cross section of 70×70×4.8 mm. The steel of the core plate and restraining tube is Grade Q235 by Chinese design code for steel structures, and its nominal Young's modulus and yield strength are 2×10^5 MPa and 235 MPa, respectively.

The numerical integration of equation of motion and numerical model updating are also carried out in the dSPACE. Firstly, the displacement of experimental substructure is calculated in dSPACE and sent to the MTS testing system. The MTS controller receives it as a measurement signal and instantly sends it to the actuator to load the specimen to the target displacement. Then the measurements of reaction force and displacement are sent by the MTS back to dSPACE. With the experimental data, the parameters of hysteretic model are estimated and used to update the numerical substructure in dSPACE. This completes one time step of numerical integration, physical loading and model updating, and these will be repeated until the end of the test.

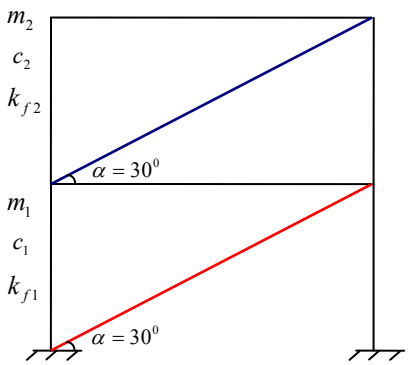

Fig. 13 Schematic of the braced frame

Fig. 14 Photograph of BRB in testing rig

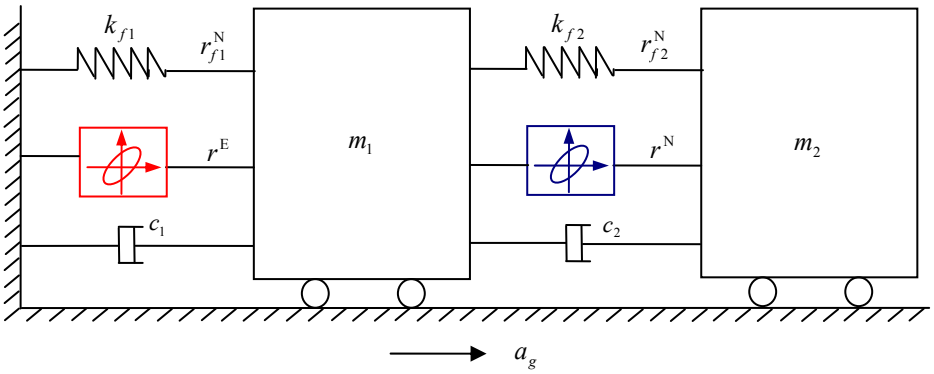

Fig. 15 Mechanical model of the two-story braced frame

The mechanical model of the braced frame can be represented by the two-degree-of-freedom system as shown in Fig. 15. The mass $m_1 = m_2 = 3\times10^6$ kg; the frame is assumed elastic and story stiffness $k_{f1} = k_{f2} = 50$ kN/mm; the calculated initial stiffness of the BRB is 130 kN/mm; the resulting structural periods are $T_1 = 1.381$s and $T_2 = 0.5275$s; Rayleigh damping is adopted and the viscous damping coefficients c_1 and c_2 are so determined that modal damping ratio $\zeta_1 = \zeta_2 = 0.02$. The seismic input is El Centro (NS, 1940) earthquake record whose peak acceleration is scaled to 100 mm/s^2. The fourth-order Runge-Kutta method is used for numerical integration with time interval of 0.01s. The loading time for one step is 0.1s, that is to say, the loading speed is scaled down to 1/10 of real time.

The Bouc-Wen model is assumed for the BRBs. The bound constraints of the parameters are $k \geq 0$, $\beta \geq 0$, $\gamma \geq -\beta$, $n \geq 1$, and $0 \leq \alpha \leq 1$. The initial values are $z = 0$, $k = 130$ kN/mm, $\beta = 0.5$, $\gamma = 0.5$, $n = 2$ and $\alpha = 0.1$. The observation noise covariance R_{k+1} is assumed 1.5 kN^2, the process noise covariance $\mathbf{Q}_k = 10^{-7}\,\mathbf{I}_6$, and the initial state estimate error covariance $\mathbf{P}_0 = \text{diag}\,(10^{-6}, 100, 10, 10, 10^{-1}, 10^{-2})$. For parameter estimation, the measurement is axial force of the BRB, and the input is measured displacement and velocity calculated from the displacement data.

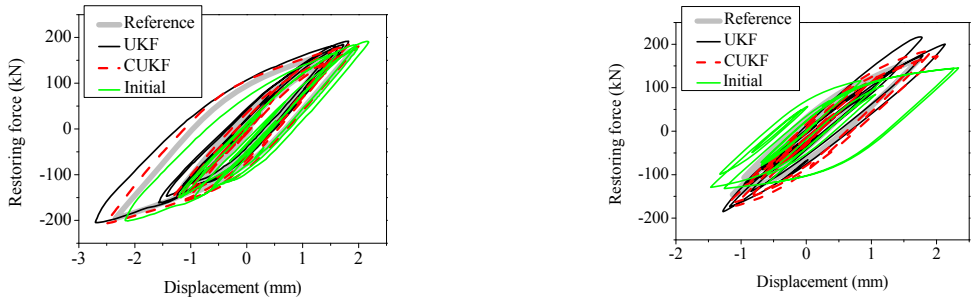

(a) Physical BRB (b) Numerical BRB

Fig. 16 Axial hysteretic loops of the physical and numerical BRBs

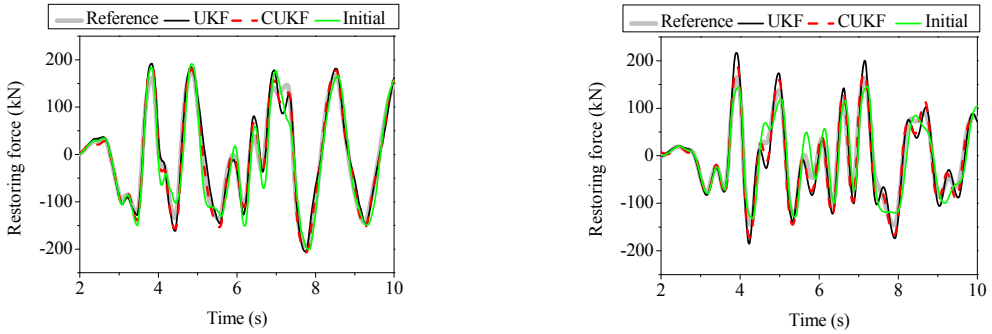

(a) Physical BRB (b) Numerical BRB

Fig. 17 Axial restoring forces of the physical and numerical BRBs

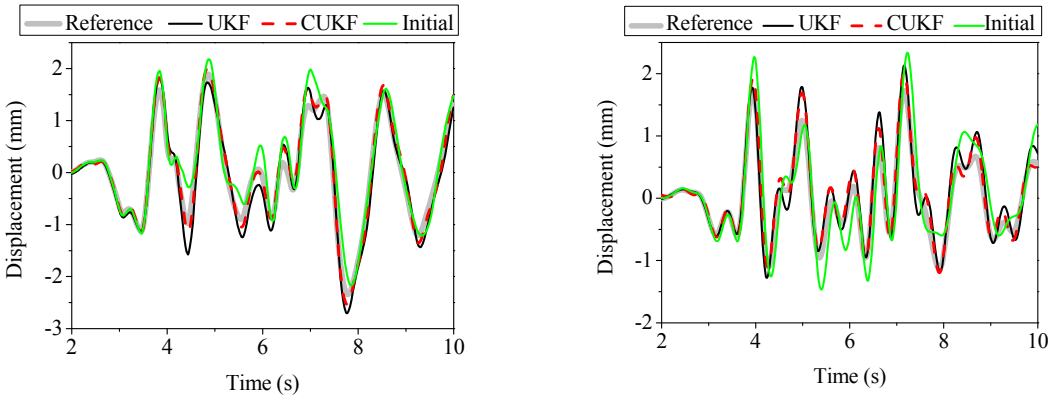

(a) Physical BRB (b) Numerical BRB

Fig. 18 Axial deformation of the physical and numerical BRBs

Table 1 RMSD of restoring forces and displacements for the physical and numerical BRB

Test type	Restoring force of BRB		Displacement of BRB	
	Physical	Numerical	Physical	Numerical
Initial	0.26	0.34	0.30	0.54
CUKF	0.12	0.20	0.14	0.25
UKF	0.19	0.28	0.23	0.34

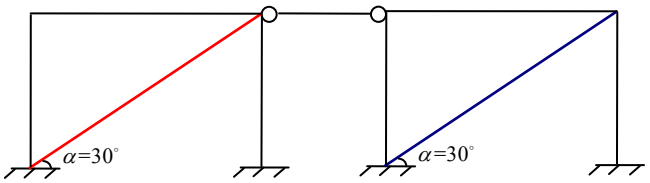

Fig. 19 Schematic of the one-story braced frame

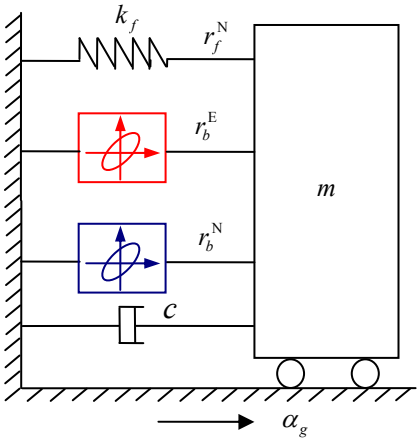

Fig. 20 Mechanical model of the one-story braced frame

Figs. 16-18 show the axial hysteretic loops, axial restoring forces, and displacements of the physical and numerical BRBs, respectively. The results denoted by "UKF" and "CUKF" are those from the model that is being updated online; those denoted by "initial" refers to the results with initial guess of parameters. The reference solutions are pure numerical results obtained using the identified parameters at the end of time histories. It is seen that the responses with fixed initial parameters deviate significantly from reference responses; the responses with CUKF are closer to the reference than those with UKF. The error indices RMSDs of the whole time histories are listed in Table 1. It is clearly seen that the errors of CUKF are less than UKF as well as those with initial parameters.

5.2 Real-time hybrid test

The test structure is two one-story frames connected by a rigid bar as shown in Fig. 19; its mechanical model is depicted in Fig. 20. The masse is $m = 3\times10^6$ kg; the total lateral stiffness of the frame is $k_f = 100$ kN/mm; damping ratio is $\zeta = 0.02$; the period of the system is $T = 0.6035$s.

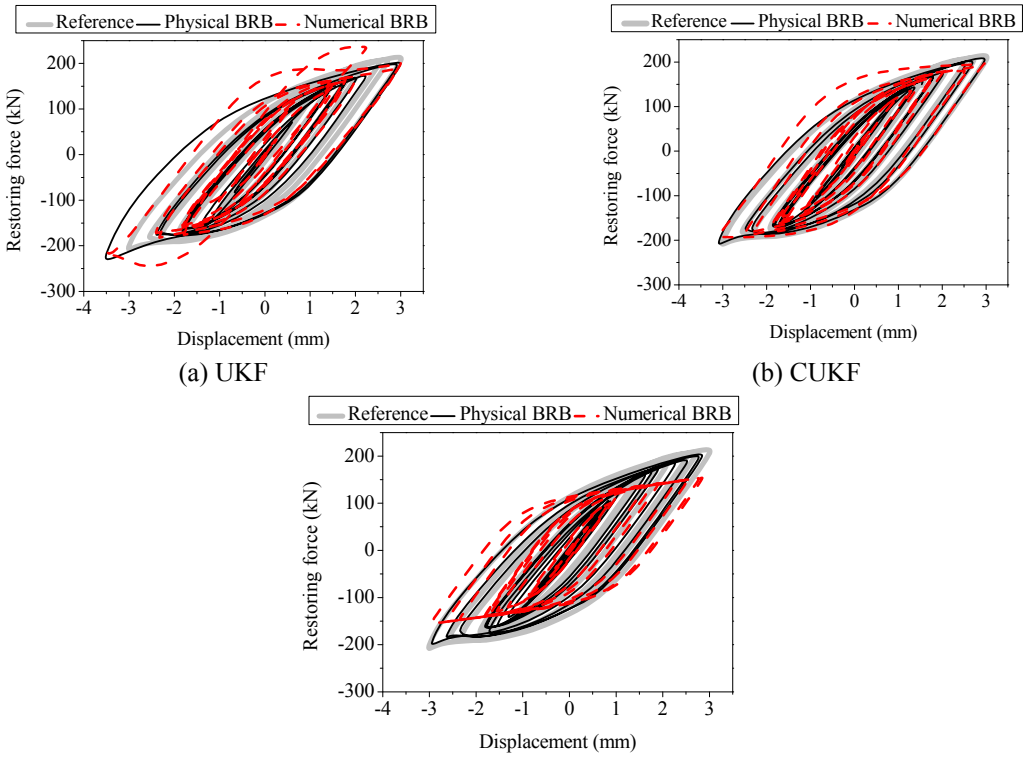

(a) UKF (b) CUKF

(c) Initial

Fig. 21 Hysteretic loops from real-time hybrid testing

Two BRBs are incorporated into the frames that are assumed elastic. One of the BRBs is taken as experimental substructure and the other as well as the frames is treated as numerical substructure. The experimental BRB, initial parameters of Bouc-Wen model of the BRBs, seismic input, and numerical integration are the same as those in last subsection. But the loading of the experimental substructure is in real time. Note that there is an actuator delay between displacement command and its realization (or measurement), and the parameters of the hysteretic model of BRB are estimated using measured displacement.

The hysteretic loops of the physical BRB and their numerical counterparts with parameters determined by different approaches are shown in Fig. 21. In this figure, "Reference" refers to the cases in which the restoring force of numerical BRB directly reads the data of experimental BRB, as if there was no numerical BRB. In other cases, the restoring force of numerical BRB is calculated with computational displacement input and estimated Bouc-Wen parameters. It is seen again that the responses by CUKF are the closest to reference solutions, and the numerical hysteretic loops with the CUKF track the experimental data best. The RMSD of numerical restoring force with CUKF is 0.55, which is less than 0.64 with UKF, and 0.69 with fixed initial parameters. The large RMSD values are probably caused by the actuator delay between displacement command (or computational displacement) and displacement realization. The delay

of the actuator is around 0.06s. If the restoring forces are calculated with measured displacements, then the RMSD are 0.0602, 0.0657, and 0.1726 for CUKF, UKF and fixed initial parameters, respectively; CUKF is still the best. It is seen that time delay has significant impact on the results of real-time hybrid simulation, and hence hybrid tests with delay compensation techniques are needed in future to validate the effect of CUKF in the cases that errors from delay are minimized.

The time histories of the restoring force of BRBs and the displacement of structure are shown in Figs. 22 and 23, respectively. It is also seen that the results of CUKF match the reference responses best in general, although the differences between different cases are not as distinguishable as in the hysteretic loops.

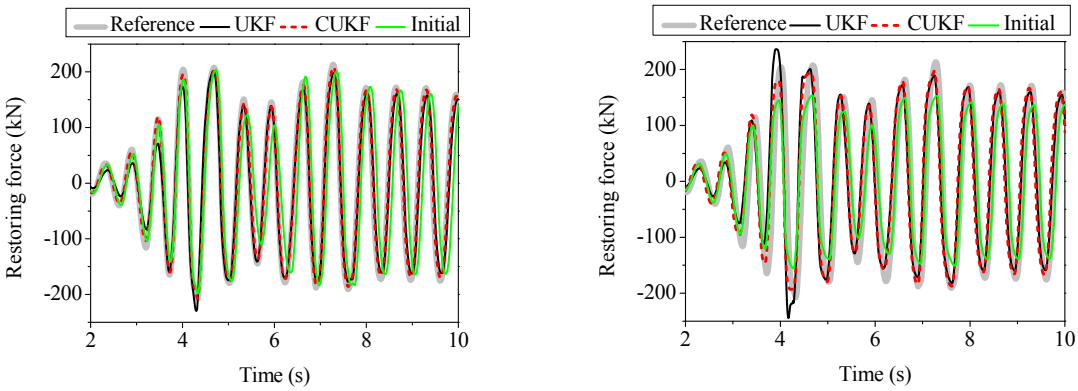

(a) Physical BRB (b) Numerical BRB

Fig. 22 Axial restoring forces of the physical and numerical BRBs

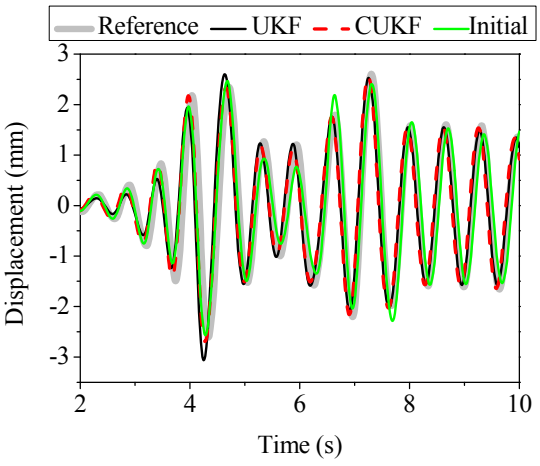

Fig. 23 Displacement response of the structure

6. Conclusions

A constrained UKF is proposed in order to improve parameter estimation. Compared to existing CUKFs, the proposed method has two improvements: (i) at prediction step, sigma points violating bound constraints are moved onto the bounds, and the relevant sigma points within the boundary are moved correspondingly to retains the symmetry for the new set of sigma points; this leads to a first-order accuracy of unscented transformation; (ii) at correction step, the state updating equation is used to generate transformed sigma points, and those transformed sigma points that violate bound constraints are projected to constraint boundary only when the updated state estimate exceeds the boundary. The effectiveness and efficiency of the proposed CUKF are validated by numerical simulation and actual hybrid tests with a BRB as experimental substructure.

Acknowledgments

The research described in this paper was financially supported by the Natural Science Foundation of China (Grants No. 51161120360 and 91315301), the Fundamental Research Funds for the Central Universities (Grant numbers: HIT. BRET2.2010009, HIT.ICRST 2010016).

References

Ahmadizadeh, M., Mosqueda, G. and Reinhorn, A. (2008), "Compensation of actuator delay and dynamics for real-time hybrid structural simulation", *Earthq. Eng. Struct. D.*, **37**(1), 21-42.

Bayer, V., Dorka, U.E., Füllekrug, U. and Gschwilm, J. (2005), "On real-time pseudo-dynamic sub-structure testing: algorithm, numerical and experimental results", *Aerosp. Sci. Technol.*, **9**, 223-232.

Bursi, O., Gonzalez-Buelga, A., Vulcan, L., Neild, S. and Wagg, D. (2008), "Novel coupling Rosenbrock-based algorithms for real-time dynamic substructure testing", *Earthq. Eng. Struct. D.*, **37**(3), 339-360.

Carrion, J. and Spencer, B. (2008), "Real-time hybrid testing using model-based delay compensation", *Smart Struct. Syst.*, **4**(6), 809-828.

Chatzi, E., Smyth, A. and Masri, S. (2010), "Experimental application of on-line parametric identification for nonlinear hysteretic systems with model uncertainty", *Struct. Saf.*, **32**(5), 326-337.

Dorka UE (2002), "Hybrid experimental-numerical simulation of vibrating structures", *Proceedings of the WAVE 2002*, Okayama, Japan.

Hashemi, M.J , Masroor, A. and Mosqueda, G. (2014), "Implementation of online model updating in hybrid simulation", *Earthq. Eng. Struct. D.*, **43**(3), 395-412.

Ikhouane, F., Maosa, V. and Rodellar, J. (2007), "Dynamic properties of the hysteretic Bouc-Wen model", *Syst. Control Lett.*, **56**(3), 197-205.

Julier, S. (2002), "The scaled unscented transformation", *Proceedings of the American Control Conference*, **6**, 4555-4559.

Jung R, Shing P(2006), "Performance evaluation of a real-time pseudodynamic test system", *Earthquake Engng Struct. Dyn.*, **35**(7),789-810.

Julier S, Uhmann J and Whyte H(2000), "A new method for the nonlinear transformation of means and covariances in filters and estimators", *IEEE Trans. Automat. Control*, **45**(3), 477-482.

Kandepu, R., Foss, B. and Imsland, L. (2008), "Applying the unscented Kalman filter for nonlinear state estimation", *J. Process Contr.*, **18**(7-8), 753-768.

Kolas, S., Foss, B. and Schei, T. (2009), "Constrained nonlinear state estimation based on the UKF

approach", *Comput. Chem. Eng*., **33**(8), 1386-1401.
Mandela, R., Kuppuraj, V., Rengaswmy, R. and Narasimhan, S. (2012), "Constrained unscented recursive estimator for nonlinear dynamic systems", *J. Process Contr.*, **22**(4), 718-728.
Mercan, O., Ricles, J., Sause, R. and Marullo, T. (2008), "Real-time large-scale hybrid testing for seismic performance evaluation of smart structures", *Smart Struct. Syst.*, **4**(5), 667-684.
Mosqueda, G., Stojadinovic, B. and Mahin, S. (2007), "Real-time error monitoring for hybrid simulation. Part Ⅱ: structural response modification due to errors", *J. Struct Eng. - ASCE*, **133**(8), 1109-1117.
Nakashima, M., Kato, H. and Takaoka, E. (1992), "Development of real-time pseudo dynamic testing", *Earthq. Eng. Struct. D.*, **21**(1), 79-92.
Simon, D. (2006), *Optimal state estimation*, John Wiley & Sons, Inc., New Jersey.
Song, W. and Dyke, S. (2013a), "Real-time dynamic model updating of a hysteretic structural system", *J. Struct. Eng. - ASCE*, 10.1061/(ASCE)ST.1943-541X.0000857.
Song, W. and Dyke, S. (2013b), "Development of a cyber-physical experimental platform for real-time dynamic model updating", *Mech. Syst. Signal Pr.*, **37**(1-2), 388-402.
Vachhani, P., Narasimhan, S. and Rengaswamy, R. (2006), "Robust and reliable estimation via unscented recursive nonlinear dynamic data reconciliation", *J. Process Contr.*, **16**(10), 1075-1086.
Wang, T. and Wu, B. (2012), "Model updating for hybrid testing with unscented Kalman filter", *Proceedings of the 7th International Workshop on Advanced Smart Materials and Smart Structures Technology ANCRiSST2012*, Bangalore, India, July, 27-28.
Wang, T., Wu, B. and Zhang, J. (2011)," Adaptive pseudo-dynamic substructure testing based on least square method", *Struct. Engineers*, **27**, 57-62. (in Chinese)
Wen, Y.K. (1976), "Method for random vibration of hysteretic systems", *J. Eng. Mech. - ASCE*, **102**(2), 249-263.
Wu, B., Wang, Q., Shing, P. B. and Ou, J. (2007), "Equivalent force control method for generalized Real-time substructure testing with implicit integration", *Earthq. Eng. Struct. D.*, **36**(9), 1127-1149.
Wu, B. and Wang, T. (2014), *Hybrid tests with buckling restrained braces for validating model updating with unscented Kalman filter*, Network for Earthquake Engineering Simulation (NEES)(distributor). Dataset. DOI: 10.4231/D3DN3ZW2R.
Yang, W.J. and Nakano, Y. (2005), "Substructure online test by using real-time hysteresis modeling with a neural network", *Proceedings of the 1st international conference on Advances in Experimental structural Engineering*, Nagaya, July 19-21.
Zhang, J. (2010), *Adaptive substructure pseudo-dynamic testing method*, M.D. Dissertation, Harbin Institute of Technology, Harbin, China, 11-32. (in Chinese)

Appendix A: Proof of accuracy of mean with symmetrically replaced sigma points

For a n-dimensional random vector $\mathbf{x} = [x_1, x_2, ..., x_n]^{\mathrm{T}}$, let $\overline{\mathbf{x}} = [\overline{x}_1, \overline{x}_2, \cdots, \overline{x}_n]^{\mathrm{T}}$ and $\mathbf{P}$ denote its mean and covariance, respectively. Below we will prove that $\overline{\mathbf{y}}_{\mathrm{CUT}}$, the approximation of the mean of another random vector $\mathbf{y}$, which is nonlinearly related to $\mathbf{x}$ through $\mathbf{y} = f(\mathbf{x})$, has accuracy of first-order with the proposed constrained unscented transformation method.

Defining $\tilde{\mathbf{x}}^{(i)}$ as the difference between the ith sigma point and the mean, i.e., $\tilde{\mathbf{x}}^{(i)} = \mathbf{x}^{(i)} - \overline{\mathbf{x}}$, we obtain the nonlinear transformation $\mathbf{y}^{(i)}$ of the point through Taylor series expansion around $\overline{\mathbf{x}}$ as

$$\mathbf{y}^{(i)} = f(\mathbf{x}^{(i)}) = f(\overline{\mathbf{x}}) + \mathbf{D}_{\tilde{\mathbf{x}}^{(i)}} f + \frac{1}{2!}\mathbf{D}^2_{\tilde{\mathbf{x}}^{(i)}} f + \frac{1}{3!}\mathbf{D}^3_{\tilde{\mathbf{x}}^{(i)}} f + \cdots \tag{A1}$$

where the operator $\mathbf{D}^k_{\tilde{\mathbf{x}}^{(i)}} f$ is defined as

$$\mathbf{D}^k_{\tilde{\mathbf{x}}^{(i)}} f = \left(\sum_{j=1}^{n} \tilde{x}_j^{(i)} \frac{\partial}{\partial x_j} \right)^k f \,|_{\mathbf{x}=\overline{\mathbf{x}}} \tag{A2}$$

We first consider the unconstrained case. Assuming κ=0.5 and with Eqs. (A1), (14)-(18), and (23), we have

$$\begin{aligned}
\overline{\mathbf{y}}_{\mathrm{CUT}} &= \sum_{i=0}^{2n} W_i \mathbf{y}^{(i)} \\
&= \frac{1}{2(n+\kappa)} f(\overline{\mathbf{x}}) + \frac{1}{2(n+\kappa)} \sum_{i=1}^{2n} \left[f(\overline{\mathbf{x}}) + \mathbf{D}_{\tilde{\mathbf{x}}^{(i)}} f + \frac{1}{2!}\mathbf{D}^2_{\tilde{\mathbf{x}}^{(i)}} f + \frac{1}{3!}\mathbf{D}^3_{\tilde{\mathbf{x}}^{(i)}} f + \cdots \right] \\
&= \frac{2n+1}{2(n+\kappa)} f(\overline{\mathbf{x}}) + \frac{1}{2(n+\kappa)} \sum_{i=1}^{2n} \left[\mathbf{D}_{\tilde{\mathbf{x}}^{(i)}} f + \frac{1}{2!}\mathbf{D}^2_{\tilde{\mathbf{x}}^{(i)}} f + \frac{1}{3!}\mathbf{D}^3_{\tilde{\mathbf{x}}^{(i)}} f + \cdots \right] \\
&= f(\overline{\mathbf{x}}) + \frac{1}{2(n+\kappa)} \sum_{i=1}^{2n} \left[\mathbf{D}_{\tilde{\mathbf{x}}^{(i)}} f + \frac{1}{2!}\mathbf{D}^2_{\tilde{\mathbf{x}}^{(i)}} f + \frac{1}{3!}\mathbf{D}^3_{\tilde{\mathbf{x}}^{(i)}} f + \cdots \right]
\end{aligned} \tag{A3}$$

Because the symmetric placement of sigma points, i.e.,

$$\tilde{\mathbf{x}}^{(i)} = -\tilde{\mathbf{x}}^{(n+i)}, \quad i = 1, 2, \cdots, n \tag{A4}$$

it follows, for any integer $k > 0$, that

$$\sum_{i=1}^{2n} \mathbf{D}^{2k+1}_{\tilde{\mathbf{x}}^{(i)}} f = \mathbf{0}_{n\times 1} \tag{A5}$$

Then Eq. (A3) can be written as

$$\overline{\mathbf{y}}_{\mathrm{CUT}} = f(\overline{\mathbf{x}}) + \frac{1}{2(n+\kappa)} \sum_{i=1}^{2n} \frac{1}{2!}\mathbf{D}^2_{\tilde{\mathbf{x}}^{(i)}} f + \frac{1}{2(n+\kappa)} \sum_{i=1}^{2n} \left[\frac{1}{4!}\mathbf{D}^4_{\tilde{\mathbf{x}}^{(i)}} f + \frac{1}{6!}\mathbf{D}^6_{\tilde{\mathbf{x}}^{(i)}} f + \cdots \right] \tag{A6}$$

The second term on the right side of the above equation can be written as

$$\begin{aligned}\frac{1}{2(n+\kappa)}\sum_{i=1}^{2n}\frac{1}{2!}\mathbf{D}^2_{\tilde{\mathbf{x}}^{(i)}}f &= \frac{1}{2(n+\kappa)}\sum_{i=1}^{2n}\left\{\frac{1}{2!}\left[\sum_{j=1}^{n}\tilde{x}_j^{(i)}\frac{\partial}{\partial x_j}\right]^2 f\,|_{\mathbf{x}=\bar{\mathbf{x}}}\right\}\\ &= \frac{1}{4(n+\kappa)}\sum_{i=1}^{2n}\left\{\sum_{j,k=1}^{n}\left[\tilde{x}_j^{(i)}\tilde{x}_k^{(i)}\frac{\partial^2 f}{\partial x_j\partial x_k}|_{\mathbf{x}=\bar{\mathbf{x}}}\right]\right\}\\ &= \frac{1}{2(n+\kappa)}\sum_{j,k=1}^{n}\left\{\sum_{i=1}^{n}\left[\tilde{x}_j^{(i)}\tilde{x}_k^{(i)}\frac{\partial^2 f}{\partial x_j\partial x_k}|_{\mathbf{x}=\bar{\mathbf{x}}}\right]\right\}\end{aligned} \tag{A7}$$

Now suppose, among first n sigma points, there are m violating bound constraints and they are denoted by l_c ($0 \le l_c \le n$, $c = 1,2,\ldots,m$, $m \le n$). Then the second term of Eq. (A6) should be replaced by

$$\begin{aligned}&\frac{1}{2(n+\kappa)}\sum_{j,k=1}^{n}\left\{\sum_{\substack{i=1\\ i\neq l_1,\ldots,l_m}}^{n}\left[\left(\sqrt{(n+\kappa)\mathbf{P}}\right)^{\mathrm{T}}_{ij}\left(\sqrt{(n+\kappa)\mathbf{P}}\right)^{\mathrm{T}}_{ik}\frac{\partial^2 f}{\partial x_j\partial x_k}|_{\mathbf{x}=\bar{\mathbf{x}}}\right]+\sum_{c=1}^{m}\left[(\theta_c)^2\left(\sqrt{\mathbf{P}}\right)^{\mathrm{T}}_{l_c j}\left(\sqrt{\mathbf{P}}\right)^{\mathrm{T}}_{l_c k}\frac{\partial^2 f}{\partial x_j\partial x_k}|_{\mathbf{x}=\bar{\mathbf{x}}}\right]\right\}\\ &=\frac{1}{2}\sum_{j,k=1}^{n}\left[\sum_{i=1}^{n}\left(\sqrt{\mathbf{P}}\right)_{ji}\left(\sqrt{\mathbf{P}}\right)^{\mathrm{T}}_{ik}\frac{\partial^2 f}{\partial x_j\partial x_k}|_{\mathbf{x}=\bar{\mathbf{x}}}\right]+\frac{1}{2(n+\kappa)}\sum_{j,k=1}^{n}\left\{\sum_{c=1}^{m}\left[(\theta_c)^2-(n+\kappa)\right]\left(\sqrt{\mathbf{P}}\right)_{jl_c}\left(\sqrt{\mathbf{P}}\right)^{\mathrm{T}}_{l_c k}\frac{\partial^2 f}{\partial x_j\partial x_k}|_{\mathbf{x}=\bar{\mathbf{x}}}\right\}\\ &=\frac{1}{2}\sum_{j,k=1}^{n}\mathbf{P}_{jk}\frac{\partial^2 f}{\partial x_j\partial x_k}|_{\mathbf{x}=\bar{\mathbf{x}}}+\frac{1}{2(n+\kappa)}\sum_{j,k=1}^{n}\left\{\sum_{c=1}^{m}\left[(\theta_c)^2-(n+\kappa)\right]\left(\sqrt{\mathbf{P}}\right)_{jl_c}\left(\sqrt{\mathbf{P}}\right)^{\mathrm{T}}_{l_c k}\frac{\partial^2 f}{\partial x_j\partial x_k}|_{\mathbf{x}=\bar{\mathbf{x}}}\right\}\end{aligned} \tag{A8}$$

Immediately, it follows

$$\bar{\mathbf{y}}_{\mathrm{CUT}} = f(\bar{\mathbf{x}})+\frac{1}{2}\sum_{j,k=1}^{n}\mathbf{P}_{jk}\frac{\partial^2 f}{\partial x_j\partial x_k}|_{\mathbf{x}=\bar{\mathbf{x}}}+\frac{1}{2(n+\kappa)}\sum_{j,k=1}^{n}\left\{\sum_{c=1}^{m}\left[(\theta_c)^2-(n+\kappa)\right]\left(\sqrt{\mathbf{P}}\right)_{jl_c}\left(\sqrt{\mathbf{P}}\right)^{\mathrm{T}}_{l_c k}\frac{\partial^2 f}{\partial x_j\partial x_k}|_{\mathbf{x}=\bar{\mathbf{x}}}\right\}+\cdots \tag{A9}$$

The exact mean $\bar{\mathbf{y}}$ obtained directly from Taylor series expansion is

$$\bar{\mathbf{y}} = f(\bar{\mathbf{x}})+\frac{1}{2}\sum_{j,k=1}^{n}\mathbf{P}_{jk}\frac{\partial^2 f}{\partial x_j\partial x_k}|_{\mathbf{x}=\bar{\mathbf{x}}}+\frac{1}{4!}E\left[\mathbf{D}^4_{\tilde{\mathbf{x}}}f\right]+\frac{1}{6!}E\left[\mathbf{D}^6_{\tilde{\mathbf{x}}}f\right]+\cdots \tag{A10}$$

Comparing Eqs. (A9) and (A10), we clearly see that the true mean and the mean calculated by the constrained unscented transformation agree each other to the first order.

Appendix B: Proof for updated covariance calculated with transformed sigma points

$$
\begin{aligned}
\mathbf{P}_{k+1|k+1} &= \mathbf{P}_{k+1|k} - \mathbf{K}_{k+1}\mathbf{P}_{yy,k+1|k}\mathbf{K}_{k+1}^{\mathrm{T}} \\
&= \mathbf{P}_{k+1|k} - \mathbf{P}_{xy,k+1|k}\mathbf{P}_{yy,k+1|k}^{-1}\mathbf{P}_{yy,k+1|k}\left(\mathbf{P}_{yy,k+1|k}^{-1}\right)^{\mathrm{T}}\mathbf{P}_{xy,k+1|k}^{\mathrm{T}} \\
&= \mathbf{P}_{k+1|k} - \mathbf{P}_{xy,k+1|k}\left(\mathbf{P}_{yy,k+1|k}^{-1}\right)^{\mathrm{T}}\mathbf{P}_{xy,k+1|k}^{\mathrm{T}} \\
&= \mathbf{P}_{k+1|k} - \mathbf{P}_{xy,k+1|k}\left(\mathbf{P}_{vy,k+1|k}^{-1}\right)^{\mathrm{T}}\mathbf{P}_{xy,k+1|k}^{\mathrm{T}} - \mathbf{P}_{xy,k+1|k}\mathbf{P}_{yy,k+1|k}^{-1}\mathbf{P}_{xy,k+1|k}^{\mathrm{T}} + \mathbf{P}_{xy,k+1|k}\mathbf{P}_{yy,k+1|k}^{-1}\mathbf{P}_{xy,k+1|k}^{\mathrm{T}} \\
&= \mathbf{P}_{k+1|k} - \mathbf{P}_{xy,k+1|k}\left(\mathbf{P}_{yy,k+1|k}^{-1}\right)^{\mathrm{T}}\mathbf{P}_{xy,k+1|k}^{\mathrm{T}} - \mathbf{P}_{xy,k+1|k}\mathbf{P}_{yy,k+1|k}^{-1}\mathbf{P}_{xy,k+1|k}^{\mathrm{T}} + \mathbf{P}_{xy,k+1|k}\mathbf{P}_{yy,k+1|k}^{-1}\mathbf{P}_{yy,k+1|k}^{\mathrm{T}}\left(\mathbf{P}_{yy,k+1|k}^{\mathrm{T}}\right)^{-1}\mathbf{P}_{xy,k+1|k}^{\mathrm{T}} \\
&= \mathbf{P}_{k+1|k} - \mathbf{P}_{xy,k+1|k}\left(\mathbf{P}_{xy,k+1|k}\mathbf{P}_{yy,k+1|k}^{-1}\right)^{\mathrm{T}} - \mathbf{P}_{xy,k+1|k}\mathbf{P}_{yy,k+1|k}^{-1}\mathbf{P}_{xy,k+1|k}^{\mathrm{T}} + \mathbf{P}_{xy,k+1|k}\mathbf{P}_{yy,k+1|k}^{-1}\mathbf{P}_{yy,k+1|k}^{\mathrm{T}}\left(\mathbf{P}_{xy,k+1|k}\mathbf{P}_{yy,k+1|k}^{-1}\right)^{\mathrm{T}} \\
&= \mathbf{P}_{k+1|k} - \mathbf{P}_{xy,k+1|k}\mathbf{K}_{k+1}^{\mathrm{T}} - \mathbf{K}_{k+1}\mathbf{P}_{xy,k+1|k}^{\mathrm{T}} + \mathbf{K}_{k+1}\mathbf{P}_{yy,k+1|k}\mathbf{K}_{k+1}^{\mathrm{T}} \\
&= \sum_{i=0}^{2n} W_{k,i}\left(\mathbf{X}_{k+1|k,i} - \hat{\mathbf{x}}_{k+1|k}\right)\left(\mathbf{X}_{k+1|k,i} - \hat{\mathbf{x}}_{k+1|k}\right)^{\mathrm{T}} + \mathbf{Q}_k - \sum_{i=0}^{2n} W_{k,i}\left[\mathbf{X}_{k+1|k,i} - \hat{\mathbf{x}}_{k+1|k}\right]\left[h(\mathbf{X}_{k+1|k,i}) - \hat{\mathbf{y}}_{k+1|k}\right]^{\mathrm{T}}\mathbf{K}_{k+1}^{\mathrm{T}} \\
&\quad - \mathbf{K}_{k+1}\sum_{i=0}^{2n} W_{k,i}\left[h(\mathbf{X}_{k+1|k,i}) - \hat{\mathbf{y}}_{k+1|k}\right]\left[\mathbf{X}_{k+1|k,i} - \hat{\mathbf{x}}_{k+1|k}\right]^{\mathrm{T}} + \mathbf{K}_{k+1}\sum_{i=0}^{2n} W_{k,i}\left[h(\mathbf{X}_{k+1|k,i}) - \hat{\mathbf{y}}_{k+1|k}\right]\left[h(\mathbf{X}_{k+1|k,i}) - \hat{\mathbf{y}}_{k+1|k}\right]^{\mathrm{T}}\mathbf{K}_{k+1}^{\mathrm{T}} \\
&\quad + \mathbf{K}_{k+1}\mathbf{R}_{k+1}\mathbf{K}_{k+1}^{\mathrm{T}} \\
&= \sum_{i=0}^{2n} W_{k,i}\left\{\left[\mathbf{X}_{k+1|k,i} - \hat{\mathbf{x}}_{k+1|k}\right] + \mathbf{K}_{k+1}\left[\hat{\mathbf{y}}_{k+1|k} - h(\mathbf{X}_{k+1|k,i})\right]\right\}\left\{\left[\mathbf{X}_{k+1|k,i} - \hat{\mathbf{x}}_{k+1|k}\right] + \mathbf{K}_{k+1}\left[\hat{\mathbf{y}}_{k+1|k} - h(\mathbf{X}_{k+1|k,i})\right]\right\}^{\mathrm{T}} \\
&\quad + \mathbf{Q}_k + \mathbf{K}_{k+1}\mathbf{R}_{k+1}\mathbf{K}_{k+1}^{\mathrm{T}} \\
&= \sum_{i=0}^{2n} \begin{matrix} W_{k,i}\left\{\left[\mathbf{X}_{k+1|k,i} + \mathbf{K}_{k+1}\left(\mathbf{y}_{k+1} - h(\mathbf{X}_{k+1|k,i})\right)\right] - \left[\hat{\mathbf{x}}_{k+1|k} + \mathbf{K}_{k+1}\left(\mathbf{y}_{k+1} - \hat{\mathbf{y}}_{k+1|k}\right)\right]\right\} \\ \left\{\left[\mathbf{X}_{k+1|k,i} + \mathbf{K}_{k+1}\left(\mathbf{y}_{k+1} - h(\mathbf{X}_{k+1|k,i})\right)\right] - \left[\hat{\mathbf{x}}_{k+1|k} + \mathbf{K}_{k+1}\left(\mathbf{y}_{k+1} - \hat{\mathbf{y}}_{k+1|k}\right)\right]\right\}^{\mathrm{T}} \end{matrix} + \mathbf{Q}_k + \mathbf{K}_{k+1}\mathbf{R}_{k+1}\mathbf{K}_{k+1}^{\mathrm{T}} \\
&= \sum_{i=0}^{2n} W_{k,i}\left\{\mathbf{X}_{k+1|k+1,i} - \left[\hat{\mathbf{x}}_{k+1|k} + \mathbf{K}_{k+1}\left(\mathbf{y}_{k+1} - \hat{\mathbf{y}}_{k+1|k}\right)\right]\right\}\left\{\mathbf{X}_{k+1|k+1,i} - \left[\hat{\mathbf{x}}_{k+1|k} + \mathbf{K}_{k+1}\left(\mathbf{y}_{k+1} - \hat{\mathbf{y}}_{k+1|k}\right)\right]\right\}^{\mathrm{T}} + \mathbf{Q}_k + \mathbf{K}_{k+1}\mathbf{R}_{k+1}\mathbf{K}_{k+1}^{\mathrm{T}} \\
&= \sum_{i=0}^{2n} W_{k,i}\left(\mathbf{X}_{k+1|k+1,i} - \hat{\mathbf{x}}_{k+1|k+1}\right)\left(\mathbf{X}_{k+1|k+1,i} - \hat{\mathbf{x}}_{k+1|k+1}\right)^{\mathrm{T}} + \mathbf{Q}_k + \mathbf{K}_{k+1}\mathbf{R}_{k+1}\mathbf{K}_{k+1}^{\mathrm{T}}
\end{aligned}
\tag{B1}
$$